CONF-921110--38

The Influence of the Rib Width on the Performance of Tubes with the Separation and Reattachment Enhancement Mechanism*

B. Arman and T. J. Rabas

Energy Systems Division
Argonne National Laboratory
9700 S. Cass Avenue
Argonne, IL 60439

ANL/CP--75904

DE93 004248

ABSTRACT

This paper presents numerically predicted turbulent heat-transfer and friction-factor results for tubes with transverse, rectangular ribs for different width-to-height ratios. The rib spacing was maintained at values where the separated flow over the rib reattached between adjacent ribs (i.e. the separation and reattachment enhancement mechanism).

The mean Nusselt number was found to decrease slightly with an increase in the width to height ratio for low Prandtl number fluids (Pr = 0.71). However, the trend is more complex for higher Prandtl number fluids. The mean Nusselt number can either increase or decrease depending on the magnitude of the Prandtl number and rib spacing. The friction factors decreased with an increase in the width to height ratio and the magnitude of this decrease was somewhat Reynolds number dependent.

---

* Work supported by the U.S. Department of Energy, Assistant Secretary for Conservation and Renewable Energy, Office of Industrial Technology, Advanced Industrial Concepts Division, under contract W-31-109-Eng-38.

Manuscript submitted for the 1992 ASME Winter Annual Meeting, November 8-13, Anaheim, CA.

INTRODUCTION

The turbulent, forced-convective heat-transfer performance of heat-exchanger tubes can be significantly increased with discrete disruptions positioned transverse or nearly transverse to the tube axis and with a spacing exceeding the reattachment length. This geometry was proposed and/or used for many single-phase forced-convection applications and fell into a mechanism category called separation and reattachment (Rabas, 1989).

Disruption Geometry Parameters

The tube geometry parameters that govern the thermal-hydraulic performance of tubes with the separation and reattachment mechanism are the disruption height, e, pitch, p, and shape. The disruption pitch and height are shown in Figure 1 which is a schematic of the turbulent flow structure between square disruptions. Manufacturing methods currently exist to make tubes with a wide range of these parameters, the major limitation is the hardness of the tube material. The major focus of previous experimental investigations was to determine the effects of the disruption height and pitch. There are prediction methods that do an adequate job to account for these two effects provided that the tubes used to generate the data base were made by the same manufacturing process and have essentially the same disruption shape. These prediction methods do not yield acceptable results when used to predict the performance of tubes made by different manufacturers and/or manufacturing processes — tubes with different disruption shapes.

The shape of the disruptions depends on the manufacturing process and can vary from gentle wavy profiles to rectangular shapes with sharp corners. For commercially-available spirally indented tubes, common shapes are arc, semicircular, and wavy. Other shapes that have been studied are rectangular, circular, trapezoidal and triangular.

The rectangular disruption shape has received considerable attention. This shape was the favorite choice for many of the early experimental investigations. In addition, the rectangular shape was preferred for many basic investigations to obtain a fundamental understanding of the enhancement mechanisms. Also, it lends itself for easy modeling in the validation of computational fluid-dynamic and heat-transfer computer codes. Because of these reasons, the effects of the width-to-height ratio of rectangular disruptions on the thermal-hydraulic performance of enhanced tubes was selected for this study.

A review of the literature dealing with the experimental results and numerical predictions that address the effect of the width-to-height ratio of rectangular disruptions is now presented. It will be demonstrated that the general trend is known but the impact on the performance cannot be properly quantified. A numerical computer program is then used to quantify this shape effect. An overview of this numerical code is presented in the Appendix.

EXISTING EXPERIMENTAL AND NUMERICAL RESULTS

Experimental results obtained with rectangular disruptions in circular passages and in rectangular and annular passages are first presented. Then some results from a numerical study are discussed.

Experimental Results — Circular Passages

Rectangular disruptions that are transverse to the flow direction — a 90 degree helix angle — have received considerable attention for circular passages (tubes). Data were obtained by Savage and Myers (1963), Sutherland and Miller (1964), Webb et al. (1971), Berger and Whitehead (1977), Berger and Hau (1979), Mendes and Mauricio (1987), and Baughn and Rody, (1992). However, none of these experimental studies focused on the

influence of width-to-height ratio on the thermal-hydraulic performance. As a result, empirical prediction methods are not available to evaluate the effect of the disruption width for flow inside circular passages.

Data comparisons were made for transverse disruptions of different shapes but not between different rectangular shapes. Some examples are the investigations of Nunner (1956), Hijikata and Mori (1987), and Kalinin et al. (1991). Of particular interest is the investigation of Kalinin et al. that addressed the effect on the thermal-hydraulic performance of the width-to-height ratio of arc-shaped disruptions. The parameter used to characterize this ratio is

$$\frac{\langle e \rangle}{e_{max}} = \frac{1}{e_{max} p} \int_0^p e(x)\, dx \tag{1}$$

where e(x) describes the axial profile variation. They showed that the friction factor always decreases with an increase of $\langle e \rangle / e_{max}$ but the heat-transfer performance was insensitive to this parameter. For a rectangular shape, $\langle e \rangle / e_{max} = (w/e)/(p/e)$. These results suggest that the friction factor decreases with an increase of the width-to-height ratio and the heat-transfer performance is independent of the width-to-height ratio.

Lewis (1975) proposed a multiple region or a discrete-element approach to predict the heat-transfer and pressure-drop performance of enhanced tubes with different shaped transverse disruptions. This method did not predict any difference in the performance resulting from different width-to-height ratios of rectangular disruptions. However, a difference was predicted with closely spaced disruptions or when the separation is less than the reattachment length. The method employed by Lewis could be refined to predict the appropriate trends if it were based on more recent information.

This review of existing data obtained with circular passages does not clearly describe the trend; therefore, it certainly does not quantify the effect of the disruption shape. However, substantially more data were obtained with annular and rectangular passages.

Experimental Data — Annular and Rectangular Passages

Rectangular disruptions with different width-to-height ratios were extensively studied when positioned inside annular and rectangular passages. They are commonly used for the external cooling of fuel element rods in gas-cooled reactors (annular passages) and for the internal cooling of gas-turbine blades (rectangular passages). Because of these applications, many of these investigations did not consider a fully enhanced passage. For annular passages, only the inner rods were enhanced. For rectangular passages, only one wall or two opposite walls were enhanced. As a result, these data can be used to determine trends but cannot be used directly for correlation development with circular passages.

First consider very wide disruptions. Bergles and Athanassiadis (1983) studied the flow over a single disruption on one wall of a rectangular channel with width-to-height ratios varying from one to ten. The downstream reattachment length was found to decrease when the width was increased from unity (square) to about five heights. At this value, the reattachment occurred on the top of the disruption and the reattachment or recirculation length measured from the back face was about three disruption heights. This investigation suggests that there will be a significant performance change for very wide disruptions where the width-to-height ratios are greater than about five. However, most of the interest — heat-exchanger tubes, gas-cooled reactor rods, and gas-turbine blades — is focused on smaller ratios or $0.25 < w/e < 2.0$ because of the reduced material and superior thermal performance.

A very active program in the 1970s was devoted to the development of prediction methods for transverse, rectangular disruptions on the outside surface of a rod placed inside a plain, outer tube. A benchmark publication by Dalle Donne and Meyer (1977), which contained a reference list of 79 publications, essentially culminated this work. The authors suggested that their prediction methods, developed mostly from annular-passage data, are applicable for internally enhanced circular passages. Because only the internal surface was enhanced, transformations are necessary to correct the annular data to the internally enhanced circular passage, the shape of interest for this investigation.

The percent errors between the friction-factor and heat-transfer prediction methods of Dalle Donne and Meyer (1977) with experimental data for internally enhanced tubes are presented in Table 1. The most important point displayed by this table is that their prediction methods are not acceptable for circular passages. Two data sources were considered: Webb et al. (1971) and Mendes and Mauricio (1987). There are other very acceptable data sources but these were considered the most representative and current. The tube geometry is characterized by three numbers such as 01/1.04/10. For this tube, e/D = 0.01, w/e = 1.04, and p/e = 10.

For the data of Webb et al. (1971), the agreement with the friction factor and the Nusselt number for air (Pr = 0.71) is acceptable only in the fully rough region (friction factor independent of the Reynolds number). However, this is not true for the 04/0.26/10 tube geometry. In addition, the agreement between the measured and predicted Nusselt numbers is not acceptable for the other fluids. One explanation is that the majority of the data used to develop these correlations were obtained with air as the test fluid. Their prediction methods are not restricted to just the fully developed region; however, they do not do a very good job in the lower Reynolds number range even for air. For the data of Mendes and Mauricio (1987), the friction factor predictions are acceptable for the entire Reynolds number range and the Nusselt number predictions are acceptable only for the

lower Reynolds number range. An explanation for the poor agreement is again the higher Prandtl number value. The comparisons presented in Table 1 clearly demonstrate that *the prediction methods of Dalle Donne and Meyer (1977) are not acceptable for transverse, rectangular disruptions inside tubes*.

The prediction methods of Dalle Donne and Meyer (1977) are next used to determine how the shape affects the thermal-hydraulic performance, the proposition being that these trends should be similar for circular and annular passage shapes. Table 2 shows that both the friction factor and the Nusselt number decrease with an increasing width-to-height ratio and that the reduction of the friction factor exceeds that of the Nusselt number. These findings are somewhat consistent with previously discussed results although the predicted change in the thermal performance is not small as suggested by Kalinin et al. (1991).

Numerical Investigation

Only one publication was discovered that addressed the impact of the disruption width on the thermal performance of an enhanced surface. Hung et al. (1987) determined the heat-transfer enhancement with a single rectangular rib inside a circular passage. The numerical model employed a finite-volume method with standard k-ε two-equation model. The effect of the disruption height, width, and Reynolds number were determined for a fixed Prandtl number, Pr = 0.7. Uniform inlet velocity and temperature profiles were assumed and a uniform tube-wall heat-flux boundary condition was selected. Very high rib heights were used where the variation of e/D was 0.125 to 0.25 which is higher than typical commercial-tube values of 0.01 to 0.06. In addition, the width-to-height ratio was outside the range of 2 to 40 that is currently used by industry.

The findings from this numerical study that are germane to the subject of this paper are the following:

1) The pressure drop increased with an increasing disruption width.

2) The heat transfer was not affected by changes in the disruption width.

Note that the first finding contradicts that obtained by the previously discussed experimental investigations; however, the increase was not large with the correction factor being $(1 + 2\ w/D)^{0.01}$.

This review suggests how the width-to-height ratio influences the pressure drop and heat transfer of enhanced tubes with transverse, rectangular disruptions. However, there is no acceptable method to quantify this impact. The next section of the paper presents some results obtained with a validated numerical computer program that does quantify these effects.

RESULTS AND DISCUSSION

A numerical modeling approach was selected to determine the friction-factor and the Nusselt number variations as a function of the Reynolds number for different disruption shapes for fixed height to diameter ratio, e/D, and pitch to height ratios, *p*/e. This numerical code was previously validated with experimental data by Arman and Rabas (1991, 1992a, 1992b) and Rabas and Arman (1992). Only minor departures from the width to height ratios used to obtain the experimental data and used for these validations will be considered in the following results and discussion.

The computer simulations were made for the following geometries. The pitch-to-height ratios, *p*/e, were 10 and 20 and the height-to-diameter ratio, e/D, was set to 0.02. For each pitch value, width-to-height ratios, w/e, of 0.5, 1.0, and 2.0 were used. A total of six different geometries are therefore considered. The local results are presented by

opening up the disruption with x/e = 0 corresponding to the leading top corner of the disruption. The axial locations of the four disruption corners are shown in Table 3.

Table 3 – Axial Locations, x/e, of the Four Corners of The Rib or Disruption

Corners	Width-To-Height Ratio , w/e		
	0.5	1.0	2.0
Leading wall-rib	-1.0	-1.0	-1.0
Leading rib top	0.0	0.0	0.0
Trailing rib top	0.5	1.0	2.0
Trailing wall-rib	1.5	2.0	3.0

Pressure Drop and Friction Factors

Figure 2 shows the friction factors versus the Reynolds number for the six different disruption geometries. Note that the friction factors decrease with an increasing disruption width. As the Reynolds number increases, the spread between friction factors values becomes slightly larger. Also, the friction factors are not strongly Reynolds number dependent because these conditions are characteristics of the fully rough region.

The normalized local wall shear stress values (skin friction coefficient) for Re ≈ 10000 are plotted in Figure 3. There is no effect of the disruption width on the skin friction in the upstream recirculation zone, on the front face, and after the main reattachment point. The disruption width affects the shear-stress distribution only in the downstream recirculation zone and hence the location of the reattachment point. The reattachment points measured from the end of the disruption are 6.21, 6.06, and 6.0 for the width ratios of 0.5, 1, and 2, respectively suggesting that there is a slight decrease in the downstream recirculation zone with increasing pitch. An enlarged portion of the Figure 3 in the vicinity of the rib shows that there is no recirculation bubble on the rib at this Reynolds number. It appears that wall shear stress at the leading edge of the rib is not effected by the width; however, the magnitude of the maximum at the trailing edge increases with an increasing width.

The normalized local pressure drop is shown in Figure 5. In contrast to the wall shear stress, the wall pressure is more sensitive to the disruption width and is altered throughout most of the domain. The wall pressure shows a sharp decrease at the leading edge; and the pressure recovery starts immediately after. This plot also demonstrates that the pressure recovery is higher for the larger disruption widths, and is the reason for the lower overall pressure drop.

The pressure drop for an orifice in a pipe should follow a similar trend, a Δp decrease with an increase of the orifice width. Idel'chik (1966) shows that that loss coefficient first decreases until w/D equals about unity and then increases. For the w/e values considered in this paper, w/D is much less than unity; therefore the friction factor follows the same trend. However, Hung et al. (1987) predicted that the pressure drop increased with an increasing disruption width for w/D values ranging from 0.25 to 10.0. Because most of w/D values exceeded the unity value, their results are not inconsistent with the findings of this paper and pressure drop results for orifices in pipes.

Heat Transfer

Figure 6 shows the mean Nusselt numbers for the lower Prandtl number fluid (Pr=0.71). Note that there is a slight decrease in the heat-transfer performance with an increasing disruption width for both pitch values. In contrast to this, the mean Nusselt number for the higher Prandtl number fluid (Pr=21.5) presented in Figure 7 shows different trends from those obtained with air. For the tube with the pitch ratio of 10, the mean heat-transfer performance increases with an increasing width; however, for the pitch ratio of 20, there is a mixed trend. It can also be seen that the effect of the disruption width on the heat-transfer performance decreases with increasing Reynolds number for both pitch values with the higher Prandtl number.

Figure 8 shows the local Nusselt numbers for the higher Pr fluid versus the axial distance for tube with the pitch ratio of 10. Note that the rib makes the dominant contribution to the total heat transferred. As a result, the mean heat-transfer performance increases with an increase of the rib width because of the increased surface area. This is not a new finding. Rabas and Arman (1992) demonstrated that an increasing Prandtl number leads to a substantial increase of the heat-transfer enhancement at the rib and for high Pr fluids, the mean thermal performance is dominated by contribution from the rib. Note also that the magnitudes of maximum values at the rib upstream face, x/e = 0, increase with increasing width. Figure 8 also shows that there are maximum values of the local Nusselt number within the downstream recirculation zone. These values are about 2.5 to 6 times smaller than the magnitude of rib maximum values and the magnitude of these maximum values decrease with an increasing rib width.

Figure 9 shows local Nusselt number variations for the larger pitch tube. In contrast to the results for the smaller pitch, the contribution from the rib is now not as dominant. In fact, the magnitudes of maximum Nusselt numbers at the rib are smaller by a factor of almost 2 to 3. However, the contribution from the downstream recirculation region is essentially unchanged. This figure shows that the downstream maximum Nusselt number values and the maximum Nusselt number values in the vicinity of the rib both decrease with an increasing width. The locations of these maximum Nusselt numbers are located at about x/e = 3.2 measured from the end of the rib within the recirculation zone. These locations are inside the recirculation region and are about three disruption heights smaller than the reattachment lengths. Again, this finding is consistent with experimental results (see Arman and Rabas, 1992a).

Figure 10 shows the local Nusselt number variation for p/e = 20 but with Pr = 0.7 (air). The contribution of the rib to the total heat transferred is not dominant and the maximum values at the rib and within the recirculation region are about the same in

magnitude. However, the reduction in the thermal performance with increasing width in the recirculation region is the major reason for the reduction of the mean thermal performance displayed in Figure 6. Also note that locations of the maximum Nusselt numbers are at axial locations of about 6, 7, and 8.5 for w/e = 0.5, 1, and 2, respectively. These three locations are closer and are about 0.5, 1, and 2 disruption heights from the reattachment point for w/e = 0.5, 1, and 2, respectively. A comparison of the results in Figures 9 and 10 show that the locations of the maximum thermal performance move closer to the reattachment point with a reduction of the Prandtl number. Note also that the locations are now dependent on the width-to-height ratio for Pr = 0.7 whereas the locations were almost independent of w/e for Pr = 21.7.

CONCLUSION

A numerical modeling was used to determine the influence on the thermal-hydraulic performance of the width-to-height ratio of transverse, rectangular disruptions inside circular passages.

The pressure drop decreases as the width increases mainly because of the larger pressure recovery that occurs after the disruption. This finding is consistent with experiment data obtained for annular passages with only the inner surface enhanced. Although not addressed in this paper, some evidence is presented which suggests that the pressure drop will increase with an increasing width for very wide disruptions because the reattachment now occurs on the top face of the rib. However, no computer runs were made with very wide disruptions because experimental data are not available for these shapes to validate the numerical model.

The predicted location of the reattachment point (the point of zero wall shear stress in the downstream recirculation region) did not appear to be strongly dependent on the width-to-height ratio for the restricted range considered for this investigation.

The influence of the width-to-height ratio on the thermal performance is more complicated. There are two locations that make major contributions to the total heat transferred: at the rib and in the downstream recirculation region. The contribution from the rib always increases when the rib width increases because of the additional surface area. However, the contribution from the downstream recirculation region apparently always decreases when the rib width increases because of the reduced turbulent kinetic energy generated by the separation and convected to the surface. To further complicate the issue, the contributions at each are dependent on the Prandtl number of the fluid. For air, the downstream recirculation region is dominant because the location of the maximum heat transfer moves downstream and closer to the reattachment point whereas the rib becomes controlling as the Prandtl number increases.

For air, the thermal performance decreases with an increasing disruption width although this reduction is small for the width-to-height ratios considered in this investigation. The major reason for the decrease is the reduction of the thermal performance in the downstream recirculation region that is controlling for low Pr fluids. For larger Pr fluids, no consistent trend exists because of the tradeoffs between the contributions from the rib and from the recirculation region. For most cases, the net effect is almost no change of the thermal performance with increasing width-to-height ratios.

APPENDIX: Turbulence Model and Numerical Method

This appendix briefly describes the turbulence model and numerical modeling approach; however, a detailed description is given by Arman and Rabas (1992a). The governing conservation laws supply the continuity equation, the momentum equations, and the energy equation. The transport equations for k and ε are used for closure of the equation set. These governing equations are presented in many publications and therefore are not repeated here. The conservation equations coupled with the k-ε equations are the common starting point for almost all the current engineering numerical modeling efforts. The turbulence model employed is a two-layer turbulence model which is briefly described below.

The two-layer model of Chen and Patel (1988) divides the flow domain into two regions: 1) a near-wall region that includes the sublayer, the buffer layer, and a small part of the turbulent core, and 2) the remainder of the fully developed turbulent core region. The standard k-ε model is used in the core region while a one-equation model is used in the near-wall region. The advantages of the near-wall one-equation model are that only the turbulent kinetic-energy equation is solved in the near-wall region and that the near-wall treatment is dependent only on the local turbulence intensity and not the wall shear stress which changes its sign.

The matching between the one-equation near-wall treatment and the two-equation standard k-ε model in the two-layer approach can be carried out along pre-selected grid lines, even for complex flows with separation. This was recommended by Chen and Patel (1988). For this application, the match boundary was selected along a grid line with y^+ values in the range of 100 to 200, which is far from the near-wall region to ensure a smooth eddy-viscosity distribution across the boundary of the two regions.

The numerical method used for this study is the finite-volume method based on the algorithm of Patankar and Spalding (1972) that solves the steady, two-dimensional axisymmetric, incompressible conservation equations for the velocity variables u, v, and for the scalar variables p, k, and ε. The scalar variables are computed and stored at the main grid locations while the velocity variables are computed and stored in their respective staggered locations.

The diffusive terms are discretized by second-order central differencing while the convective terms are discretized by quadratic-upstream scheme (QUICK) of Leonard (1979). The velocity-pressure coupling is achieved through the use of the continuity equation applying the SIMPLEC algorithm (Van Doormaal and Raithby, 1984). The resulting algebraic equations were solved by using a line-by-line, three-diagonal matrix algorithm that sweeps in both directions.

The boundary conditions at the wall are the usual no-slip conditions; i.e, $u = v = k = 0$. There is no need to specify the wall boundary condition for ε. The wall boundary condition for the temperature is a constant wall heat flux. The axisymmetry conditions are used for the symmetry axis.

Periodicity conditions are used at the inlet and the outlet of the flow domain in order to represent a fully developed flow field. The domain length is equal to one rib pitch. Fully developed flow requires identical inlet and outlet profiles for the velocities, turbulent kinetic energy, and turbulent energy dissipation. The driving force for the flow is a constant pressure difference that exists between the inlet and outlet pressure distributions. As with the pressure profiles, the temperature profiles must be identical at the axial increments of one pitch except for a constant value displaced by an amount of $\Delta T = Q/mc_p$. For more information on the periodicity boundary conditions and the fully developed flow constraint see Patankar et al. (1977).

The first near-wall grid point is located well within the laminar sublayer ($y^+ \approx 0.1$) for all of the iterations. The number of non-uniform r-grids and non-uniform x-grids were always larger than 50. The iteration dependency tests were performed and the iterations were continued until the normalized mass residual (total mass residuals divided by the total mass flow rate) falls below 10^{-5}. The number of maximum iterations were 5000 for the momentum field; however, the maximum number of iterations for the temperature field were set to be 13000. The typical run times were about 6 to 8 hours on an IBM RS/6000-320 workstation.

NOMENCLATURE

c_p	specific heat
D	tube inside diameter
e	rib height
f	friction factor, $f = \Delta p/(\rho U^2/2)$
h	mean heat-transfer coefficient
h(x)	local heat-transfer coefficient
k	turbulent kinetic energy
k	thermal conductivity
m	total mass flow rate
Nu	mean Nusselt number, $Nu = hD/k$
Nu(x)	local Nusselt number, $Nu(x) = h(x)D/k$
p	pressure
p	disruption or rib pitch
Pr	Prandtl number, $Pr = c_p\mu/k$
Q	total heat transferred for one pitch of tube length
Re	Reynolds number based on tube diameter, $Re = \rho DU/\mu$
u	time average axial velocity component
U	average axial velocity
v	time average radial velocity component
w	disruption width
x	axial distance
y	radial distance from the wall
y^+	dimensionless distance from wall, $y^+ = \frac{y}{\nu}\sqrt{\frac{\tau_w}{\rho}}$

Greek Letters

ε	turbulent energy dissipation
μ	viscosity
ν	diffusivity
ρ	density
τ_w	wall shear stress
Δp	pressure drop for one pitch of tube length
ΔT	mean temperature drop for one pitch of tube length

REFERENCES

Arman, B. and T.J. Rabas, 1992a, Argonne National Laboratory unpublished information.

Arman, B. and T.J. Rabas, 1992b, "Disruption Shape Effects on the Performance of Enhanced Tubes with the Separation and Reattachment Mechanism," paper to be presented at the National Heat Transfer Conference, San Diego, August 9-12, 1992.

Arman, B. and T.J. Rabas, 1991, "Prediction of the Pressure Drop in Transverse, Repeated-Rib Tubes with Numerical Modeling," Fouling and Enhancement Interactions, ASME HTD-Vol. 164, pp. 93-99.

Baughn, J.W. and J. Rody, 1992, "Enhanced Turbulent Heat Transfer in Circular Ducts with Transverse Ribs,"paper to be presented at the National Heat Transfer Conference, San Diego, August 9-12, 1992.

Berger. F.P., and K.F., F.L. Hau, 1979, "Local Mass/Heat Transfer Distribution on Surfaces Roughened with Small Square Ribs," International Journal of Heat and Mass Transfer, Vol. 22, pp. 1645-1656.

Berger, F.P., and A.W. Whitehead, 1977, "Fluid Flow and Heat Transfer in Tubes with Internal Square Rib Roughening," Journal of British Nuclear Energy Society, Vol. 16, No. 2, pp. 153-160.

Bergles, G., and N. Athanassiadis, 1983, "The Flow Past a Surface-Mounted Obstacle," Transactions of ASME, Journal of Fluids Engineering, Vol. 105, pp. 461-463.

Chen, H.C., and V.C. Patel, 1988, "Near-Wall Turbulence Models for Complex Flows Including Separation," AIAA Journal, Vol. 26, pp. 641-648.

Dalle Donne, M., and L. Meyer, 1977, "Turbulent Convective Heat Transfer From Rough Surfaces With Two-Dimensional Rectangular Ribs," International Journal of Heat and Mass Transfer, Vol. 20, pp. 583-620.

Hijikata K., and Y. Mori, 1987, "Fundamental Study of Heat Transfer Augmentation of Tube Inside Surface by Cascade Smooth Surface-Turbulence Promoters," Wärme-und Stoffubertragung, Vol. 21, 115-124.

Hung, Y.H., T.M. Liou, and Y.C. Syang, 1987, "Heat Transfer Enhancement of Turbulent Flow in Pipes with an Internal Circular Rib," Advances in Enhanced Heat Transfer-1987, ASME HTD-Vol. 68, pp. 55-64.

Idelichik, I.E., 1966, Handbook of Hydraulic Resistance, Coefficients of Local Resistance and of Friction, AEC-tr-6330, p. 140.

Kalinin, E.K., G.A. Dreitser, N.V. Paramonov, A.S. Myakochin, A.I. Tikhonov, S.G. Zakirov, E.S. Levin, and L.S. Yanovsky, 1991, "Comprehensive Study of Heat Transfer Enhancement in Tubular Heat Exchangers," Experimental Thermal and Fluid Science, Vol. 4, pp. 656-666.

Leonard, B.P., 1979, "A Stable Accurate Corrective Modeling Procedure Based on Quadratic Upstream Interpolation," Computer Methods in Applied Mechanics and Engineering, Vol. 19, pp. 59-98.

Lewis, M.J., 1975, "An Elementary Analysis for Predicting the Momentum and Heat Transfer Characteristics of a Hydraulically Rough Surface," Transactions of ASME, Journal of Heat Transfer, Vol. 97, pp. 249-254.

Mendes, P.R.S., and M.H.P. Mauricio, 1987, "Heat Transfer, Pressure Drop and Enhancement Characteristics of the Turbulent Through Internally Ribbed Tubes," Convective Transport, ASME Symposium Series, HTD-Vol. 82, pp. 15-22.

Nunner, W., 1956, "Heat Transfer and Pressure Drop in Rough Tubes," VDI-Forschungsheft 455, Series B, Vol 22; A.E.R.E. Lib/Trans. 786 (1958).

Patankar, S.V., C.H. Liu, and E.M. Sparrow, 1977, "Fully Developed Flow and Heat Transfer in Ducts Having Streamwise-Periodic Variations of Cross-Sectional Area," Transactions of ASME, Journal Heat Transfer, Vol. 99, pp. 180-186.

Patankar, S.V., and Spalding, D.B., 1972, "A Calculation Procedure for Heat, Mass and Momentum Transfer in Three-Dimensional Parabolic Flows," International Journal of Heat and Mass Transfer, Vol. 15, pp. 1787-1806.

Rabas T.J. and B. Arman, 1992, Argonne National Laboratory, unpublished information.

Rabas, T.J., 1987, "Data and Correlation Review of the Enhancement for Steam Condensation on Spirally Indented Tubes," Boiling and Condensing Heat Transfer, ASME HTD-Vol. 85, pp. 97-106.

Savage, D.W., and J.E. Myers, 1963, "The Effect of Artificial Surface Roughness on Heat and Momentum Transfer," AIChE Journal, Vol. 9, No. 5, pp. 694-702.

Sutherland, W.A., and C.W. Miller, 1964, "Heat Transfer to Superheated Steam-II, Improved Performance with Turbulent Promoters," USAEC Report, GEAP-4749.

Van Doormaal, J.P., and Raithby, G.D., 1984, "Enhancements of the SIMPLE Method for Predicting Incompressible Fluid Flows," Numerical Heat Transfer, Vol. 67, pp. 147-163.

Webb, R.L., E.R.G. Eckert, and R.L. Goldstein, 1971, "Heat Transfer and Friction in Tubes with Repeated-Rib Roughness," International Journal of Heat and Mass Transfer, Vol. 14, pp. 601-617.

Data Source	Tube Geometry	Quantity	Prandtl Number	Reynolds Number 6000	10000	20000	40000	70000
Webb et.al. (1971)	01/1.04/10	f	-	-31.54	-52.17	10.87	9.05	6.31
		Nu	0.71	19.24	-5.38	21.82	14.65	10.99
		Nu	5.10	75.04	24.83	44.23	35.18	38.53
		Nu	21.70	132.13	51.30	68.03	61.69	68.02
	02/0.52/10	f	-	-18.02	26.49	14.69	15.86	15.86
		Nu	0.71	12.96	24.85	13.67	8.50	9.71
		Nu	5.10	19.44	38.74	36.84	40.87	50.79
		Nu	21.70	52.86	75.73	70.79	71.47	78.44
	04/0.26/10	f	-	46.62	47.40	46.57	43.41	42.49
		Nu	0.71	37.72	33.55	28.08	23.57	20.71
		Nu	5.10	46.53	44.77	42.73	45.05	40.01
		Nu	21.70	76.38	74.25	73.12	74.91	78.68
	02/0.52/20	f	-	-52.15	31.68	16.93	13.13	12.21
		Nu	0.71	-12.31	24.03	15.90	10.83	11.05
		Nu	5.10	-3.39	38.02	35.19	36.02	42.23
		Nu	21.70	27.81	78.60	73.37	74.07	82.50
	02/0.52/20	f	-	-36.88	17.22	26.25	24.24	20.59
		Nu	0.71	5.26	26.24	23.90	23.29	25.60
		Nu	5.10	20.21	45.37	44.23	46.44	55.54
		Nu	21.70	62.29	91.45	85.84	85.50	94.88
Mendes and Mauricio (1987)	05/1.0/8	f	-	-19.27	-18.54	-18.42	-18.42	-18.42
		Nu	2.5	3.59	10.84	17.88	48.79	85.13
	05/1.0/10	f	-	-20.80	-20.00	-19.87	-19.87	-19.87
		Nu	2.5	14.55	9.74	11.41	44.22	73.79
	05/1.0/12	f	-	-23.94	-23.24	-22.96	-22.96	-22.96
		Nu	2.5	20.08	16.32	15.92	53.62	81.56
	05/1.0/15	f	-	-31.83	-31.69	-31.55	-31.55	-31.55
		Nu	2.5	-	7.64	11.71	54.32	88.16

Table 1 – The Percent Errors Obtained with a Comparison of Experimental Data and the Dalle Donne and Meyer (1977) Prediction Methods

Data Source	Tube Geometry	Pr	Quantity	Re	0.25	0.5	1.0	2.0
Webb et.al. (1971)	01/10	0.71	f	6000	.0370	.0227	.0089	.0089
				10000	.0497	.0387	.0310	.0256
				20000	.0520	.0410	.0334	.0280
				40000	.0523	.0413	.0337	.0282
			Nu	6000	50.31	40.37	26.87	26.43
				10000	85.58	76.24	68.83	62.92
				20000	151.06	136.28	124.64	115.42
				40000	260.08	236.59	218.11	203.47
	01/20	0.71	f	6000	.0089	.0089	.0089	.0089
				10000	.0325	.0269	.0226	.0194
				20000	.0349	.0293	.0250	.0219
				40000	.0352	.0296	.0253	.0221
			Nu	6000	26.99	26.54	26.14	25.81
				10000	70.33	64.39	59.40	55.27
				20000	127.06	117.78	110.06	103.79
				40000	221.97	207.26	195.02	185.09
Mendes and Mauricio (1987)	05/8	2.5	f	6000	.1347	.0913	.0666	.0489
				10000	.1354	.0919	.0672	.0495
				20000	.1354	.0920	.0673	.0496
				35000	.1354	.0920	.0673	.0497
			Nu	6000	170.22	145.88	128.40	113.11
				10000	246.34	212.77	188.71	167.66
				20000	404.97	353.27	316.28	284.01
				35000	777.84	530.76	478.81	433.65
	05/15		f	6000	.0785	.0601	.0478	.0395
				10000	.0791	.0607	.0484	.0401
				20000	.0793	.0608	.0485	.0402
				35000	.0793	.0608	.0486	.0402
			Nu	6000	137.48	123.39	112.39	103.85
				10000	201.24	181.86	166.76	155.04
				20000	335.56	305.83	282.73	264.82
				35000	505.91	464.22	431.94	534.90

Table 2 - Effect of the Width to Height Ratio on the Friction Factor and Heat Transfer Based on the Prediction Methods of Dalle Donne and Meyer (1977)

Figure 1 – Turbulent Flow Structure within an Enhanced Tube with the Separation and Reattachment Mechanism

Figure 2 – Friction Factors as a Function of Reynolds Number

Figure 3 – Wall Shear Stress Variation for the $p/e = 20$ Tube Geometry

Figure 4 – Wall Shear Stress Variation in the Vicinity of the Rib for the $p/e = 20$ Tube Geometry

Figure 5 – Wall Pressure Drop Variation for the $p/e = 20$ Tube Geometry

Figure 6 – Mean Nusselt Numbers as a Function of Reynolds Number for Pr = 0.71

Figure 7 – Mean Nusselt Numbers as a Function of Reynolds Number for Pr = 21.5

Figure 8 – Local Nusselt Number Variation for Re ≈ 9700, Pr = 21.5 and the $p/e = 10$ Tube Geometry

Figure 9 – Local Nusselt Number Variation for Re ≈ 9700, Pr = 21.5 and the $p/e = 20$ Tube Geometry

Figure 10 – Local Nusselt Number Variation for Re ≈ 9700, Pr = 0.71 and the $p/e = 20$ Tube Geometry

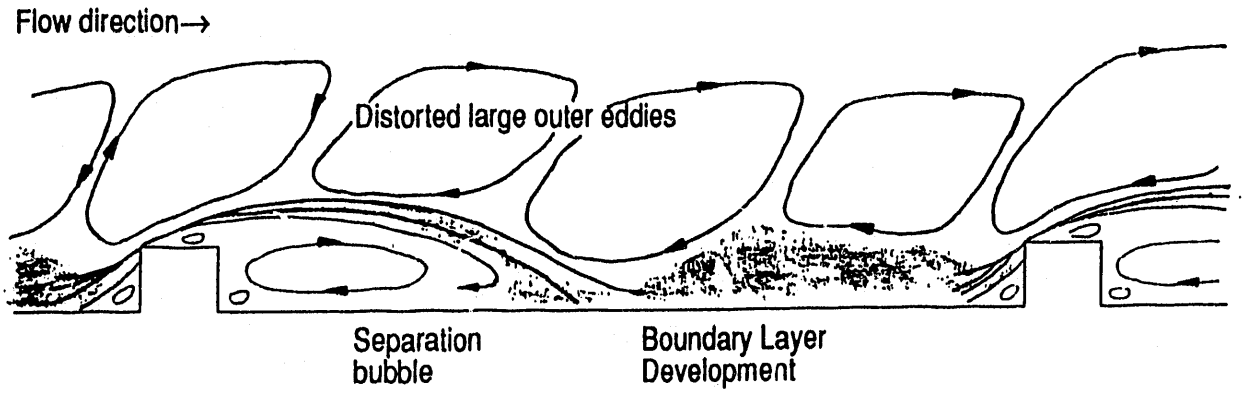

Figure 1 – Turbulent Flow Structure within an Enhanced Tube with the Separation and Reattachment Mechanism

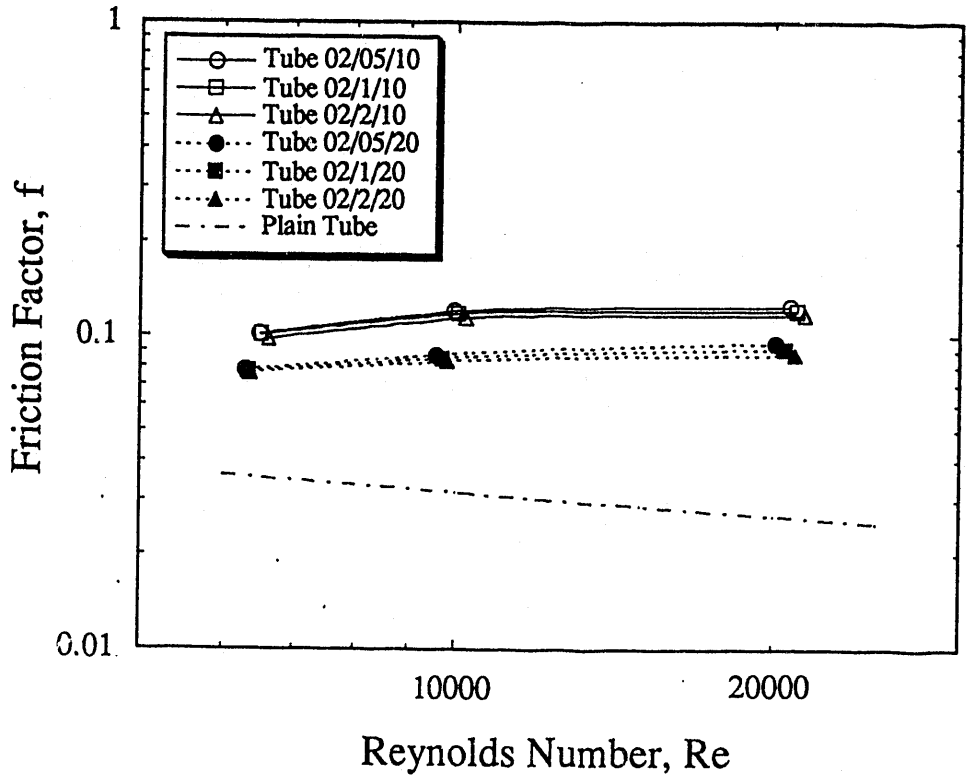

Figure 2 – Friction Factors as a Function of Reynolds Number

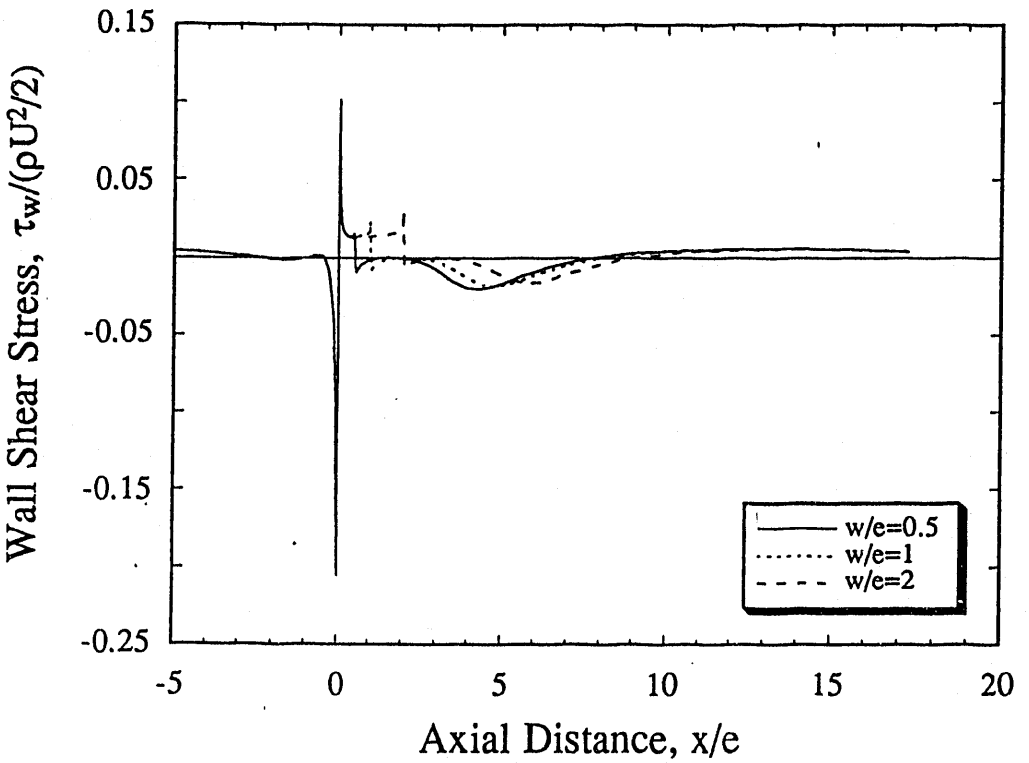

Figure 3 – Wall Shear Stress Variation for the *p*/e = 20 Tube Geometry

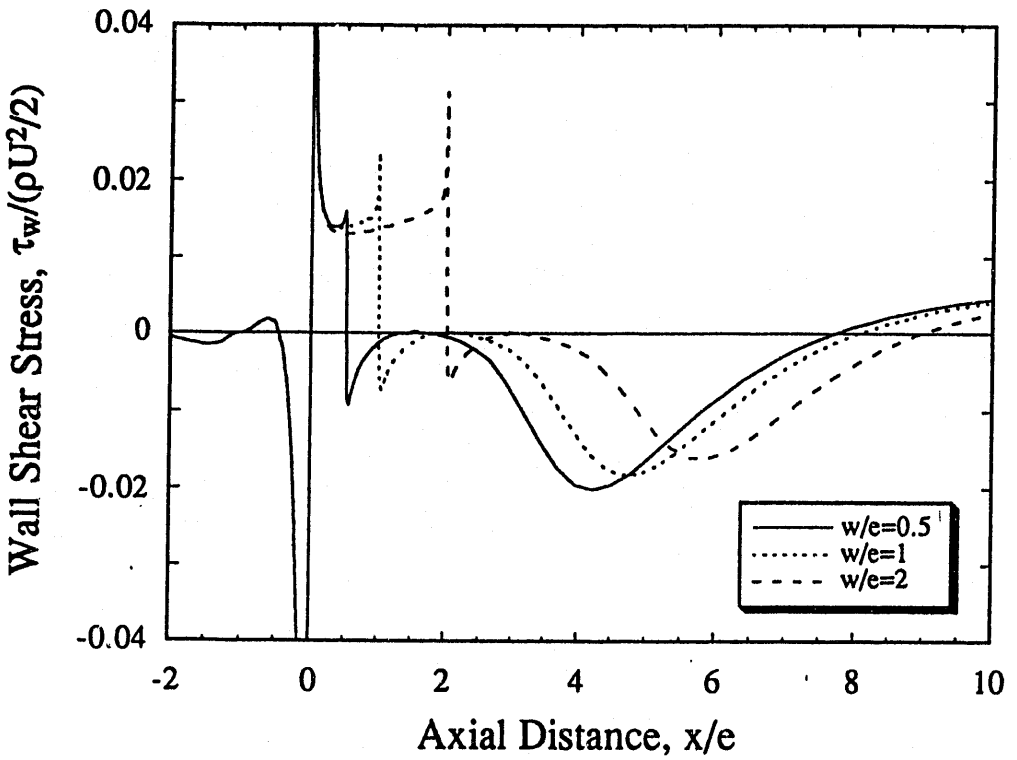

Figure 4 – Wall Shear Stress Variation in the Vicinity of the Rib for the *p*/e = 20 Tube Geometry

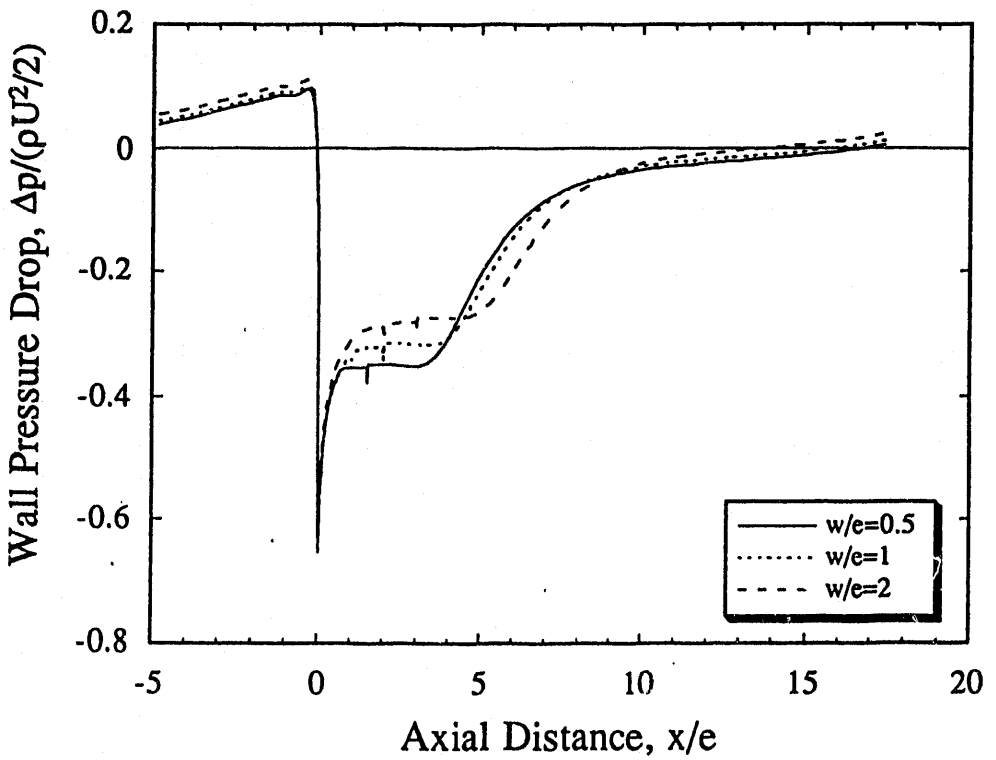

Figure 5 – Wall Pressure Drop Variation for the *p*/e = 20 Tube Geometry

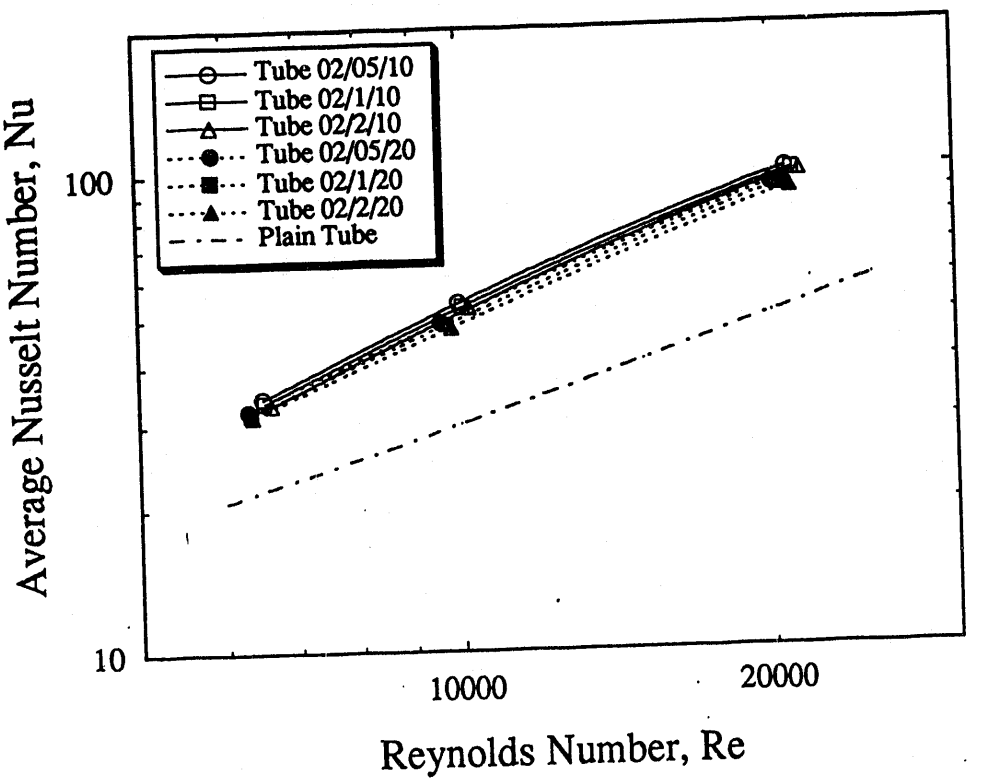

Figure 6 – Mean Nusselt Numbers as a Function of Reynolds Number for the Pr = 0.71

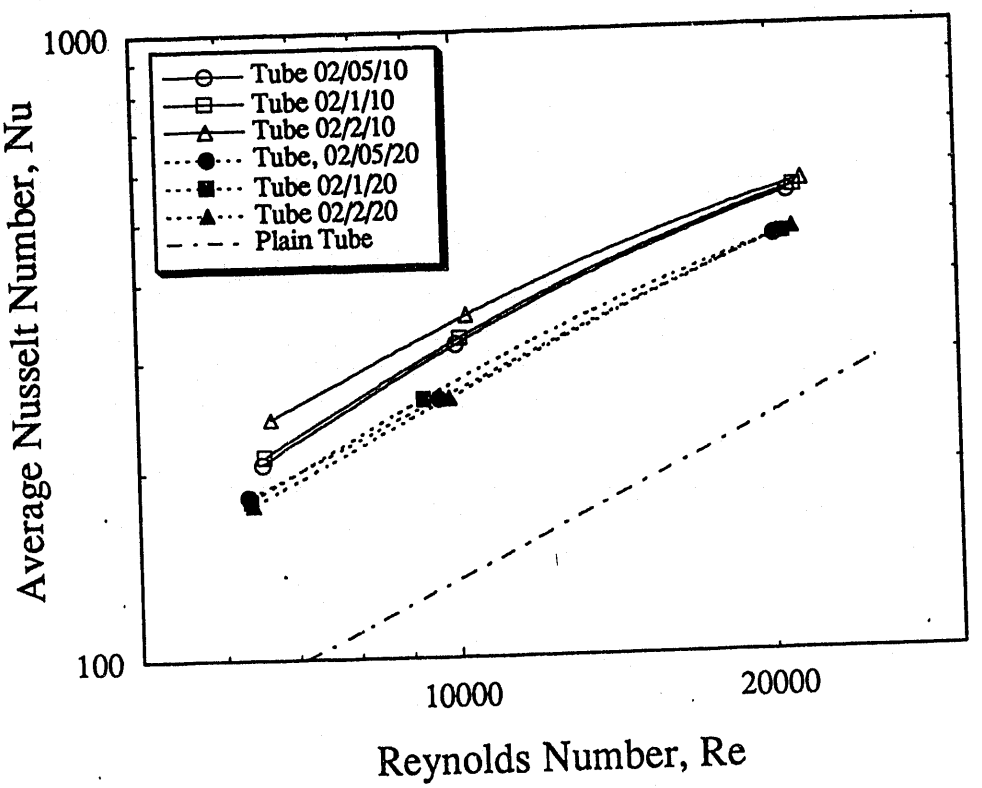

Figure 7 – Mean Nusselt Numbers as a Function of Reynolds Number for the Pr = 21.5

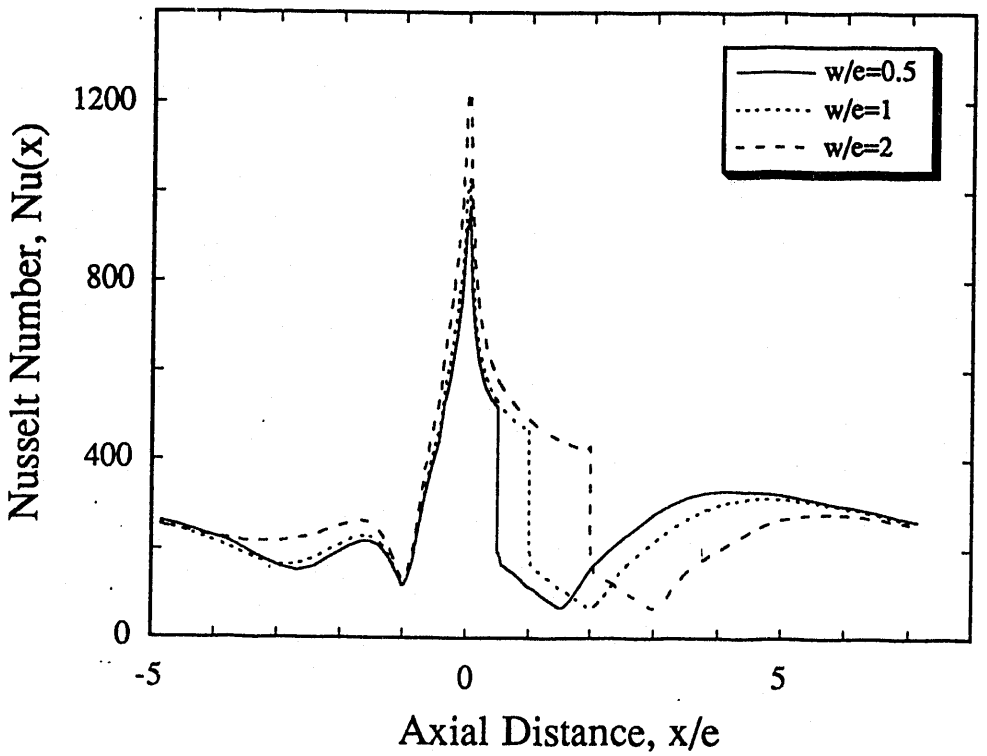

Figure 8 – Local Nusselt Number Variation for Re ≈ 9700, for Pr = 21.5 and the *p*/e = 10 Tube Geometry

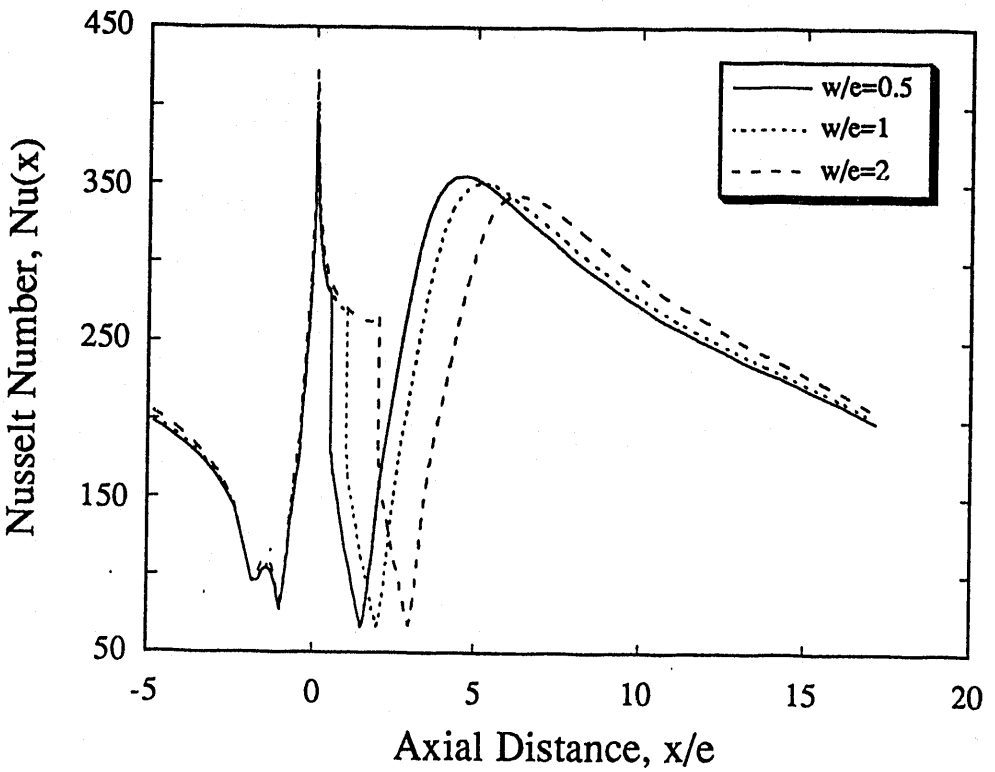

Figure 9 – Local Nusselt Number Variation for Re ≈ 9700, for Pr = 21.5 and the *p*/e = 20 Tube Geometry

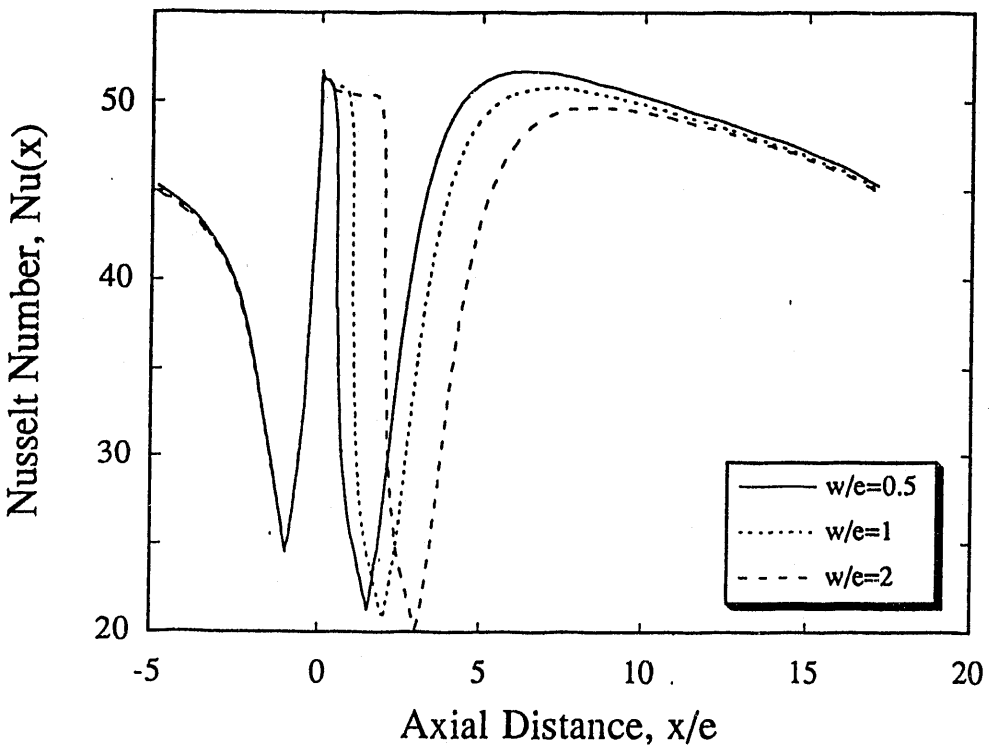

Figure 10 – Local Nusselt Number Variation for Re ≈ 9700 for Pr = 0.71 and the $p/e = 20$ Tube Geometry

END

DATE FILMED

3/29/93